ISSN 1063-7826, Semiconductors, 2020, Vol. 54, No. 11, pp. 1445–1449. © Pleiades Publishing, Ltd., 2020.
Russian Text © The Author(s), 2020, published in Fizika i Tekhnika Poluprovodnikov, 2020, Vol. 54, No. 11, pp. 1225–1229.

SEMICONDUCTOR STRUCTURES, LOW-DIMENSIONAL SYSTEMS, AND QUANTUM PHENOMENA

Dependence of the Electrophysical Characteristics of Metal–Ferroelectric–Semiconductor Structures on the Field-Electrode Material

M. S. Afanasiev[a], D. A. Belorusov[a], D. A. Kiselev[a,b], A. A. Sivov[a], and G. V. Chucheva[a,*]

[a] *Kotelnikov Institute of Radioengineering and Electronics, Fryazino Branch, Russian Academy of Sciences, Fryazino, Moscow oblast, 141190 Russia*

[b] *National University of Science and Technology "MISiS", Moscow, 119049 Russia*

**e-mail: gvc@ms.ire.mssi.ru*

Received June 8, 2020; revised July 13, 2020; accepted July 13, 2020

Abstract—Films of the composition $Ba_{0.8}Sr_{0.2}TiO_3$ (BST 80/20) are synthesized on a silicon substrate by the method of the high-frequency sputtering of a polycrystalline target. The results of investigations of the film composition, the electrophysical properties of capacitor structures based on them, and the dependence of these properties on the material (Al, Cu, Ni, Cr) of the upper electrode are presented.

Keywords: metal–dielectric–semiconductor structures, ferroelectric films of $Ba_{0.8}Sr_{0.2}TiO_3$ composition, microstructure, electrophysical properties

DOI: 10.1134/S1063782620110032

1. INTRODUCTION

Nonvolatile memory is the basic component of modern computers, digital cameras, mobile phones, or smartphones [1]. The difference between modern approaches to the development of nonvolatile memory is the use of new physical principles of information storage. One of the most relevant in the research context for future devices using nonvolatile memory is FeRAM (ferroelectric random-access nonvolatile memory or ferroelectric nonvolatile memory with random access to cells) [2]. The operating principle of FeRAM is based on a change in the polarization of a ferroelectric film, which leads to the opening or closing of a conductive channel in the metal–ferroelectric–semiconductor (MFEP) structure. The advantage of MFEP structures is the ability to vary the surface potential of the semiconductor by only controlling the polarization, thereby implementing the operations of reading, writing, or deleting information [3].

The quality of the metal–ferroelectric and ferroelectric–semiconductor interfaces determines the shape of the C–V characteristic of the MFEP structure [4, 5], and, therefore, the controllability of the semiconductor surface potential. Therefore, it is important to understand how the material of the metal field electrode affects the properties of interphase boundaries and, thus, the electrophysical characteristics of MFEP structures. This study is devoted to investigating these problems.

2. TECHNOLOGY OF PRODUCING MFEP STRUCTURES AND THEIR STRUCTURAL INVESTIGATIONS

For the investigations, we fabricated MFEP structures representing a metallic upper electrode, a $Ba_{0.8}Sr_{0.2}TiO_3$ (BST) ferroelectric film, and a (100) silicon substrate of p-type conductivity. The ferroelectric film (330 ± 15) nm thick was deposited onto the silicon substrate by the high-frequency sputtering of a polycrystalline target in an oxygen atmosphere using a Plasma-50SE installation (Russia). The film-deposition process included two stages. At the first stage, the synthesis process was carried out in oxygen, which continued for 20 min. The substrate temperature during synthesis was maintained at (620 ± 5)°C. The second stage consisted of heat treatment of the film in an oxygen atmosphere. For this purpose, the high-frequency (HF) generator was turned off, the vacuum valve was closed, and the oxygen pressure in the chamber was increased to 10^4 Pa. Further, the sample was cooled to room temperature for 2 h.

To control the quality of the BST ferroelectric film, we investigated the elemental composition by the Rutherford backscattering (RBS) of He^+ ions (energy of $E_0 = 1.6$ MeV) in an experimental installation of the analytical ion-beam complex Sokol-3 [6, 7].

We analyzed the experimental RBS spectrum recorded in the course of investigating the BST film and the theoretical RBS spectrum obtained as a result

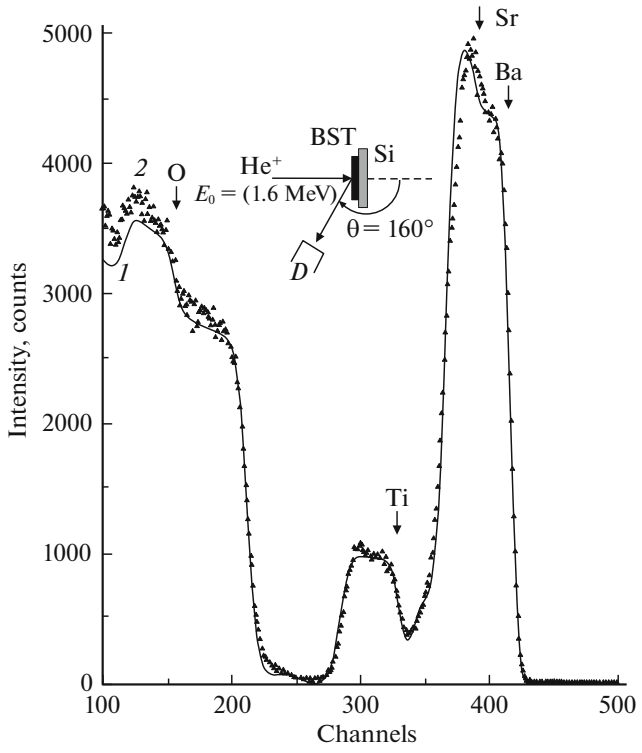

Fig. 1. (*1*) Theoretical and (*2*) experimental RBS spectra of He^+ ions (E_0 = 1.6 MeV) for the BST film. Arrows mark the energy of ion scattering at atomic nuclei located on the sample surface. Division value is 3.2 keV/channel.

of approximation using the RUMPP computer program [8]. The analysis showed that the RBS spectrum of the film contains atoms of barium (Ba), strontium (Sr), titanium (Ti), and oxygen (O) (Fig. 1). The approximation required a theoretical RBS spectrum in the form of the spectrum of a two-layer structure with slightly different layer compositions. The RBS spectrum itself consists of two peaks in the high-energy region, a stepwise rise in scattering, and an additional peak at the step in the diagram under observation. The energies corresponding to the scattering of helium ions at atomic nuclei located on the surface of the sample under study are indicated by the corresponding arrows.

The first high-energy peak in the spectrum is associated with the scattering of ions at the nuclei of Ba and Sr atoms. The next peak reflects the presence of Ti atoms in the BST film. The step in the spectrum is the result of ion scattering at the nuclei of silicon (Si) of the substrate. The peak observed at the step is associated with scattering at oxygen nuclei. The distribution of elements in two layers into which we had to divide the film to obtain satisfactory approximation is presented in Table 1.

We determined the BST-film thickness using an SU5000 scanning electron microscope (SEM). The SEM image of a BST-film cleavage taken at an angle of 45° is shown in Fig. 2a. From this, we found a film thickness of (330 ± 15) nm.

The surface of thin BST films was visualized in the contact scanning mode on an Ntegra Prima atomic-force microscope (AFM) (NT-MDT, Russia) using a CSG10/Pt cantilever. The BST-film structure was characterized by an average grain size of ~(40–75) nm and a root-mean-square (rms) surface roughness of ~4 nm (Fig. 2b). The BST film was morphologically uniform; there were no extraneous contaminants and inclusions on the film surface.

To investigate the electrophysical properties of the structures, the upper electrodes were formed on the surface of the ferroelectric film, which were deposited by the electron-beam method through a shadow mask on an A700QE/DI12000 installation (Germany). The area of the electrodes was ~2.7×10^{-4} cm^2, and the thickness was (0.1 ± 0.01) μm. Samples of four types were obtained depending on the electrode material—copper (Cu), nickel (Ni), chromium (Cr), and aluminum (Al).

3. EXPERIMENTAL RESULTS AND DISCUSSION

The C–V characteristics and the dielectric-loss tangent tanδ were measured using an automated experimental installation [9] by an Agilent E4980A precision LCR meter.

In Fig. 3, we show the C–V characteristics $C(V_g)$ of the MFEP structures measured at room temperature at a frequency of 100 kHz and normalized to the highest value C_{max} of the capacitance. The samples were supplied with a bias voltage V_g from –20 to +20 V and vice versa at a field-sweep rate of 0.75 V/s.

The dependences of the capacity of the MFEP structures on the bias voltage were in the form of a hys-

Table 1. Distribution of elements in the BST film obtained as a result of theoretical approximation of the RBS spectrum of He^+ ions

Layer number	Thickness, nm	Element content, at %				
		Ba	Sr	Ti	O	Note
1	170	0.78	0.23	0.97	3.2	–
2	150	0.75	0.27	1.03	3.3	The presence of Si is possible, ~0.15

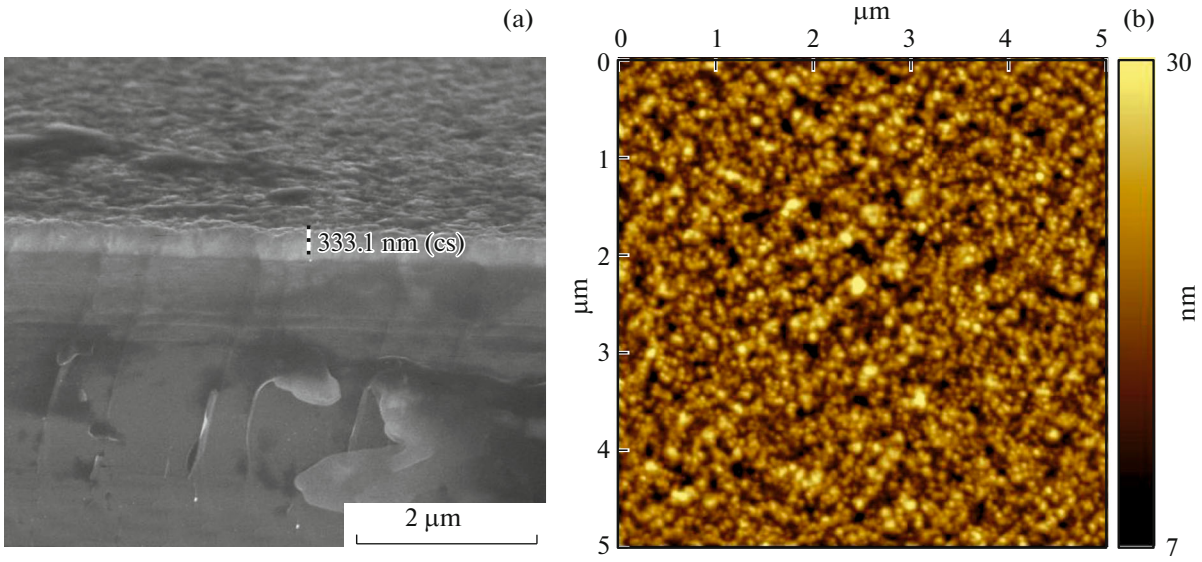

Fig. 2. Images of the BST film obtained by (a) SEM and (b) AFM.

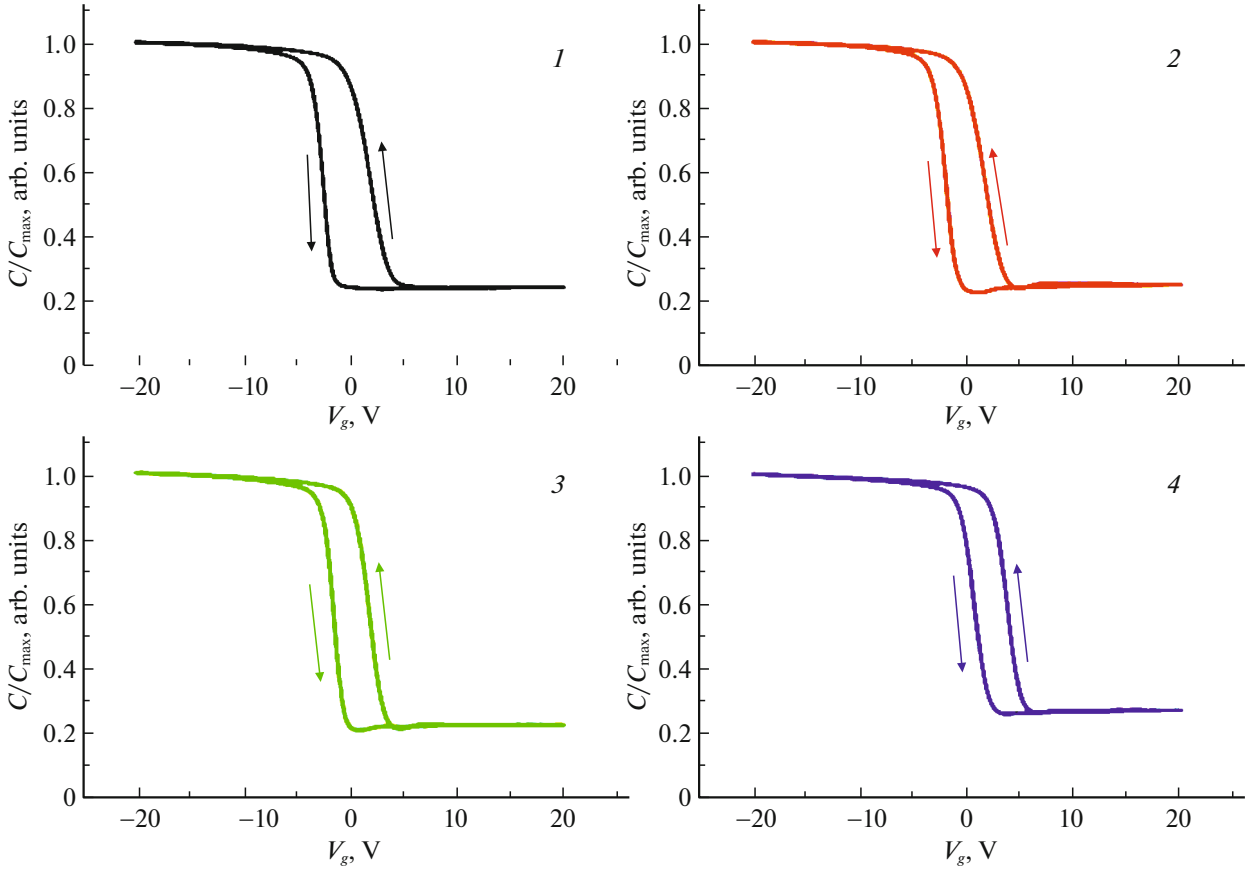

Fig. 3. *C–V* characteristics of MFEP structures measured at a frequency of 100 kHz at room temperature. Upper electrode: (*1*) Al, (*2*) Cu, (*3*) Ni, and (*4*) Cr.

Table 2. Values of the ratio of the maximum sample capacity to the minimum one and the width of the $C-V$-characteristic hysteresis loop depending on the material of the upper electrode

Electrode	Ratio of the maximum capacity to the minimum one	Loop width, V	Electrode	
			work function, eV [11]	specific resistance, 10^{-8} Ω m [12]
Al	4.18	4.5	4.21	2.8
Cu	4.56	4	4.36	1.75
Ni	5.11	3.6	4.95	8.7
Cr	3.85	3.3	4.60	2.7

teresis loop with a width from 3.3 V (Cr) to 4.4 V (Al) (see Table 2) depending on the material of the field electrode of the sample. It is known [10] that the $C-V$ characteristics should be shifted relative to each other along the abscissa by a value equal to the difference between the work functions of the corresponding metals for structures with the same dielectric and substrate parameters differing only in terms of the materials of the upper electrode; i.e., this shift should not exceed 0.74 V for this case (see Table 2). Here, a shift of the $C-V$ characteristics of >3 V was observed; this may be due to the presence of built-in charge in the ferroelectric film and charge due to both structural defects in BST and surface states at the interphase boundaries. The most pronounced and asymmetric shift of the characteristic (+2.7 V) was observed for the structure with a field electrode made of Cr. When comparing the experimental $C-V$ characteristics of the samples with different materials of the field electrode both in the slope of the characteristic, its symmetry, and in the width of the hysteresis loop, the structures with a Ni electrode were most attractive.

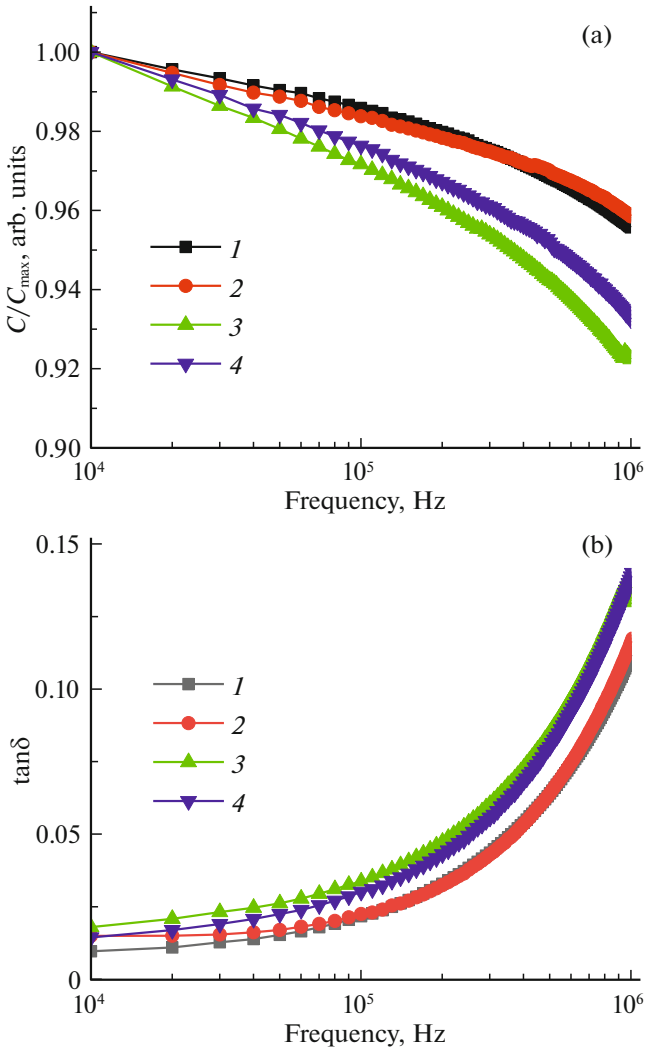

Fig. 4. Frequency dependences of (a) the capacity and (b) the dielectric-loss tangent of MFEP structures. Upper electrode: (*1*) Al, (*2*) Cu, (*3*) Ni, and (*4*) Cr.

Table 2 lists the values of certain parameters of the characteristics of the MFEP structures obtained as a result of processing the measured $C-V$ characteristics. The highest value (5.11) of the ratio of the maximum sample capacity to the minimum value was observed for the structure with a Ni electrode, and the lowest ratio (3.85), for the structure with the Cr electrode.

In Fig. 4, we show the frequency dependences of the capacity (Fig. 4a) and the dielectric loss tangent (Fig. 4b) of the MFEP structures measured at room temperature and the constant bias voltage $V_g = -20$ V. For all samples, the capacity values decreased with increasing frequency. The largest drop in capacity was observed in the structure with the Ni electrode, and the smallest, in the structure with the Cu electrode.

The frequency dependences of the dielectric-loss tangent for the MFEP structures were identical and showed an increase with frequency. In the frequency range of 10–80 kHz, the curves were almost parallel to the abscissa axis, and in the range of 80–1000 kHz, they turned into a sharp increase. The tangent of the dielectric-loss angle was ~0.02 in the frequency range of 10–80 kHz and increased to ~0.14 in the range of 80–1000 kHz.

In Fig. 5, we show the plotted temperature dependences of the capacity at $V_g = -20$ V for measurements of the $C-V$ characteristics of the MFEP structures at a frequency of 100 kHz. The $C-V$ characteristics were measured in the temperature range from 22°C to 125°C.

With increasing temperature, a decrease in the capacity of all the structures was observed. The measurements performed showed that the structures with

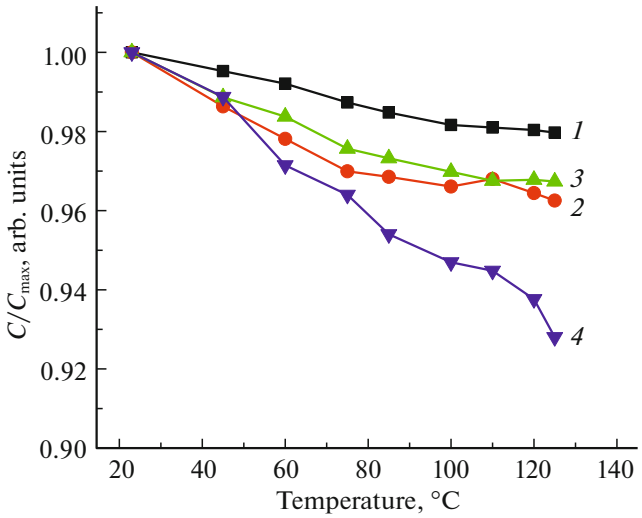

Fig. 5. Plotted temperature dependence of the sample capacity at $V_g = -20$ V when measuring the $C-V$ characteristics. Upper electrode: (*1*) Al, (*2*) Cu, (*3*) Ni, and (*4*) Cr.

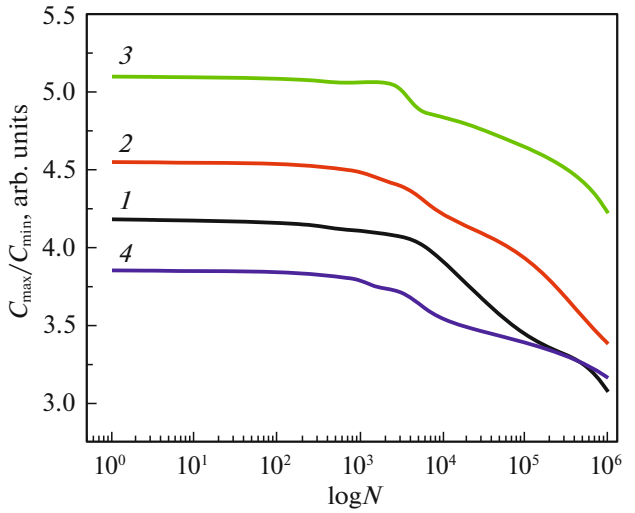

Fig. 6. Dependence of the ratio of the maximum sample capacity (C_{max}) to the minimum one (C_{min}) on the number of switching cycles. Upper electrode: (*1*) Al, (*2*) Cu, (*3*) Ni, and (*4*) Cr.

Al, Cu, and Ni electrodes are more thermally stable than the structures with Cr electrodes.

In Fig. 6, we show the dependences of the ratio of the maximum capacity of the MFEP structures to the minimum capacity on the number of switching cycles. The samples were cyclically supplied with a bias voltage V_g from -20 to $+20$ V. The test was carried out with 10^6 switching cycles.

It is shown that, the values of C_{max}/C_{min} did not change after 3×10^3 cycles of switching of the MFEP structures. After 3×10^3 and up to 10^6 switching cycles, the values of the ratios of the maximum sample capacity to the minimum one changed for all structures practically the same, but by no more than 15%. It is planned that further investigations of the changes in these ratio values for the number of switching cycles exceeding 10^6 will be conducted. The results will be reflected in further studies.

4. CONCLUSIONS

The investigations carried out showed that the structures represent the features of behavior of the considered materials from which the contact pads are made. Thus, for each material of the field electrode, its own niche can be determined when fabricating MFEP structures and devices based on them for a new generation of the element base of modern electronics taking into account the cost of materials and the manufacturability. For example, instead of using expensive and technologically complex rare-earth metals, it is possible to use a combination of well-known and technologically advanced materials.

FUNDING

This study was carried out within the framework of the state assignment and was partially supported by the Russian Foundation for Basic Research, project nos. 18-29-11029, 19-07-00271, and 19-29-03042.

CONFLICT OF INTEREST

The authors declare that they have no conflicts of interest.

REFERENCES

1. Y. Yao, C. Li, Z. L. Huo, M. Liu, C. X. Zhu, C. Z. Gu, X. F. Duan, Y. G. Wang, L. Gu, and R. C. Yu, Nat. Commun. **4**, 1 (2013).
2. H. Ishiwara, J. Nanosci. Nanotechnol. **12**, 7619 (2012).
3. A. Chanthbouala, A. Crassous, V. Garci, K. Bouzehouane, S. Fusil, X. Moya, and A. Barthélémy, Nat. Nanotechnol. **7**, 101 (2012).
4. Z. Wen, C. Li, D. Wu, A. Li, and N. Ming, Nat. Mater. **12**, 617 (2013).
5. Z. Xi, J. Ruan, C. Li, C. Zheng, Z. Wen, J. Dai, and D. Wu, Nat. Commun. **8**, 1 (2017).
6. L. C. Feldman and D. W. Mayer, Fundamentals of Surface Thin Film Analysis (North-Holland, Amsterdam, 1986).
7. V. K. Egorov and E. V. Egorov, NBIKS—Nauka Tekhnol., No. 3, 29 (2019).
8. L. R. Doolittle, Nucl. Instrum. Methods Phys. Res., Sect. B **9**, 344 (1985).
9. E. I. Gol'dman, A. G. Zhdan, and G. V. Chucheva, Instrum. Exp. Tech. **40**, 841 (1997).
10. S. M. Sze and K. Ng. Kwok, *Physics of Semiconductor Devices* (Wiley, New York, 2007).
11. https://infotables.ru/fizika/132-rabota-vykhoda-elektronov-izmetallov-tablitsa#hcq=XKemm0s. https://infotables.ru/fizika/132-rabota-vykhoda-elektronov-izmetallov-tablitsa.
12. https://zygar.ru/mineraly/metal/resistance-of-metals.html.

Translated by V. Bukhanov